Ibn Al-Haitham Journal for Pure and Applied Sciences
Journal homepage: jih.uobaghdad.edu.iq
PISSN: 1609-4042, EISSN: 2521-3407
IHJPAS. 2025, 38(3)

# Modeling of Moth Eye Structures for Silicon Solar Cells Efficiency Enhancement

**Ethar S. Jasim[1], Imad H. Khaleel [2*] and Ali F. Al-Shawabkeh[3]**
[1,2]Department of Physics, College of Education for Pure Science (Ibn Al-Haitham), University of Baghdad, Baghdad, Iraq.
[3]Department of Scientific Basic Sciences, Faculty of Engineering Technology, Al-Balqa Applied University, Amman, Jordan.
*Corresponding Author.

Received: 9 June 2024 Accepted:7 October 2024 Published: 20 July 2025
**doi.org/10.30526/38.3.4028**

## Abstract
Moth-eye nano-structure is essentially used as a light-trapping technique for more efficient and cost-effective solar cells. This computational study investigated two dimensions of rectangular silicon base anti-reflected nanostructure for ultra-thin film solar silicon cell efficiency enhancement. The introduced simulation procedure depends on numerical methods and Lumerical software. Impacts of the structure geometry, which was the width and height, on optical and electrical properties were investigated. It found that the geometry of the structure has a significant effect on the absorption and reflection spectrum, due to structure light-trapping effects, and the maximum absorption increases in visible regain reported at a width of 300 nm and height of 100 nm. We also determined the fill factor, short circuit current, and open circuit voltage. It is found that the short circuit current density is significantly influenced by the structure geometry due to a change in absorption, which influences electron-hole generation. It’s also found that the performance can be enhanced by choosing a suitable dimension for the suggested structure. The optimum efficiency enhancement achieved was from 8.71% to 11.89%, and the obtained results are encouraging for using the presented procedure to design more complex structures.
**Keywords:** Moth-Eye, Nano structures, Solar cells, Finite difference time domain, Efficiency enhancement.

## 1. Introduction
The world has faced an existential threat due to the continuous population increases and finite natural resources. Conversely, the pollution associated with the increased consumption of fossil energy sources has led to climate change (1-4). Sustainable energy is required to combat these risks, and solar energy is the most promising. Today. silicon solar cells represent 90% of photovoltaic cells because of their high operational stability, nontoxicity, and abundance (5-8).
However, getting good absorption throughout a wide range of solar spectrum requires a considerable amount of silicon material with a topical cell thickness of roughly 180-300 µm,

which raises the production cost, so one possible solution to minimize the cost is ultra-thin silicon solar cell with thickness in few micrometers due to needing less material and protection cost and it has a lot of interest recently (9-15).

Ultra-Thin Film Solar Cell UTFSC has lower efficiency because of decreasing silicon thickness, and surface, bulk recombination. As a result, both experiential and theoretical work established several light trapping techniques to minimize the reflection on the surface and maximize the absorption of light to enhance the UTFSC efficiency, such as surface texturing, anti-reflected coating, diffraction grating, metallic nanoparticles (16-25).

In this study, we establish a computational model based on the FDTD combined with a Lumerical-Charge solution that has been utilized to investigate alternative designs of silicon-based like moth eye nanostructure for lowering solar cell production costs and improved efficiency.

## 2. Materials and Methods

Solar cells' efficiency depends on the design and optical and electrical material properties. For the optical simulation, the absorption of silicon solar cells' active layer per unit volume is defined by (26):

$$Pabs = -0.5w\,|E|^2\,imag\,(\mathcal{E})$$

(1)

where $|E|$ is the electric field, $w$ is the angular frequency, and $imag\,(\mathcal{E})$ represents a permittivity imaginary part.

Dividing absorption energy per unit volume by the energy per photon ($\hbar\omega$), one can calculate the photon generation rate (27).

$$\mathrm{g} = \frac{Pabs}{\hbar\omega} = \frac{-0.5\mathrm{w}\,|\boldsymbol{E}|^2\,\mathrm{imag}\,(\mathcal{E})}{\hbar}$$

(2)

Where ħ is a reduced Planck's constant. The integration of (g) over the whole spectrum, which is considered in this study $(300-1100nm)$ determines the photon generation rate. If we consider an ideal case, the current length unit $(A/m)$ can be expressed as (28):

$$I = e\,\mathrm{g}$$

(3)

Where $e$ is the charge on an electron

Solar cell quantum efficiency can be defined as (29):

$$QE\,(\lambda) = \frac{Pabs(\lambda)}{Pin(\lambda)}$$

(4)

Where Pin $(\lambda)$ and Pabs $(\lambda)$ are the powers of the incident and absorbed photons at a wavelength $(\lambda)$ respectively.

The following equations yield the ideal short-circuit current density $J_{sc(ideal)}$ (30):

$$J_{sc(ideal)} = e\int \frac{\lambda}{\hbar c}\mathrm{Q}E(\lambda)\,I_{AM1.5}(\lambda)d\,\lambda \tag{5}$$

Where c denotes the speed of light in free space, $I_{AM1.5}$ denote considered solar irradiance.

The solar cell open-circuit voltage can be defined as (31):

$$V_{oc} = \frac{AKT}{q}\,ln\left(\frac{I_L}{I_o}+1\right) \tag{6}$$

Where; $T$ is the temperature, $K$ represents the Boltzmann constant, $q$ is the electron charge, $I_L$ is the light saturation current, and $I_o$ is the dark saturation current, and A is the solar ideality factor.

The current density $\mathrm{J}_{sc}$ can be expressed as (28):

$$J_{sc} = qG(L_n + L_P) \tag{7}$$

Where G is the generation rate, and $L_n$ and $L_P$ are the electron and hole diffusion lengths, respectively

The fill factor $FF$ gauges a solar cell's J-V properties is given by (32):

$$FF = \frac{V_{max} \times J_{max}}{V_{oc} \times J_{sc}} \tag{8}$$

The output power, or maximum power, can be stated as:

$$P_{max} = V_{oc} \times J_{sc} \times FF \tag{9}$$

Finally, the efficiency of a solar cell can be expressed as (33):

$$\eta = FF \times V_{oc} \times J_{sc}/S_{AM1.5G} \tag{10}$$

where $S_{AM1.5G}$ It is the incident power.

Modeling solar cells as a device requires both optical and electrical simulations. **Figure (1.a)** represents a two-dimensional schematic diagram for ultra-thin film silicon solar cells with a Moth-Eye nano-structure array, where the front contact (emitter) and rear contact (base) are made of Silver (Ag), and Aluminum (Al), respectively. R represents the external loud. Also, the optical and electrical simulation regions are shown. **Figure (1.b)** represents the optical simulation diagram established by FDTD simulation. A planer wave light source was employed, and both the reflection and transmitting were monitored by an R-monitor and T-monitor below, and above the solar cell respectively. The left and right are set to be periodic boundary conditions (PBC) meanwhile, the upper and bottom sides are set to be perfectly matched layers (PML). The geometry of moth-eye array units is set to be rectangular where w and h represent the width and height respectively while d represents the distances between two structures, and the material of the structure is silicon.

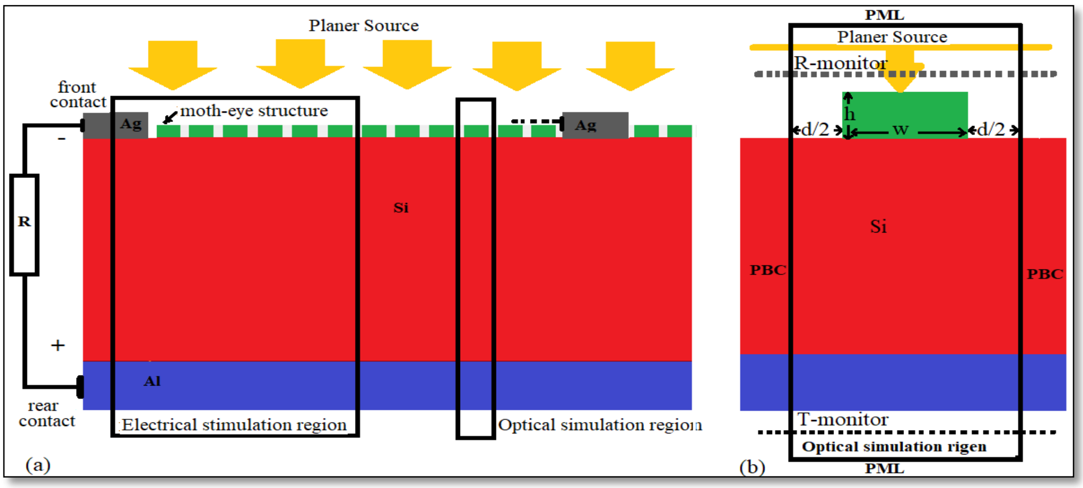


**Figure 1.** (a) Solar cell with rectangular moth-eye structure, electrical and optical simulation regions. (b) The optical simulation region unites cells.

The device simulation was done in three steps as shown in **Figure (2)**, in the first step optical properties (Reflection, Absorption, Transmission), heat, and electrical generation profile within the active region of the silicon solar cell over the entire incident solar spectrum were computed by FDTD-Lumerical software employing Equation (1) and Equation (2), for a given incident planer wave in the study frequency range (300-1100nm), after import optical martial properties for the active region of solar cell and proposed moth-eye structure(34). Further, the ideal circuit current can be calculated using Equation (5). The second step, which represents thermal simulation, the heat generation profile was computed from the first step then the heat energy was calculated from the absorbed photon which has energy above the bandgap energy of solar active martial. In the third step, the optical and heat generation profile is imported from the last two steps, then a voltage sweep is carried out to obtain current-voltage characteristics and power-voltage curve of the modulated solar cell. So, the open-circuit voltage $V_{oc}$, current density $J_{sc}$, fill factor FF, maximum power $P_{max}$, and the solar cell efficiency $\eta$ calculated by employing Equation (6, 7, 8, 9, 10) respectively.

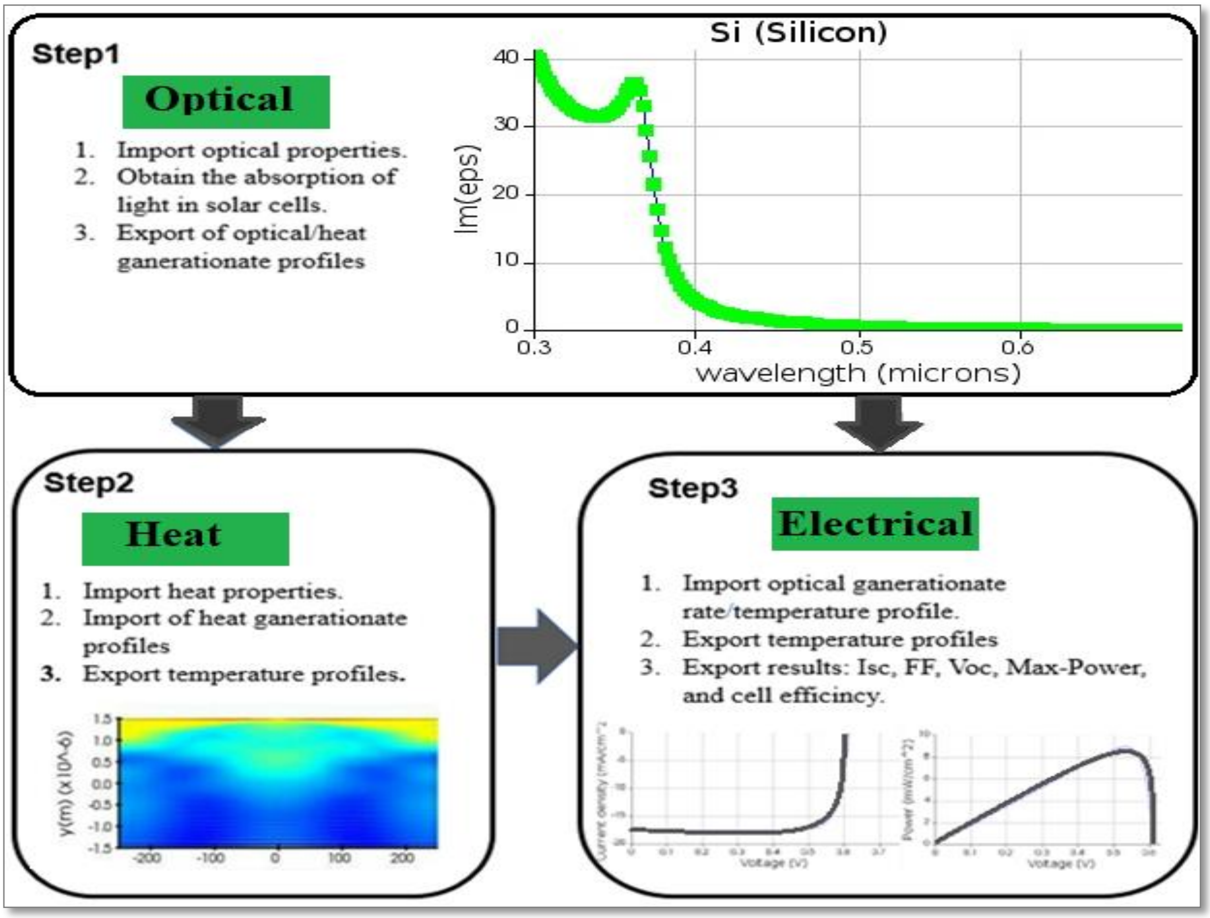


**Figure 2.** Three simulation steps: optical, heat, and electrical.

## 3. Results and Discussion

To study the effects of the suggested moth-eye structure on the silicon solar cell performance, four subwavelength widths were considered for the rectangular structure ($w = 100, 200, 300, 400\ nm$), and for each width value of the rectangle, there were nine values for the structure height ($h = 50, 100, 150, 200, 250, 300, 350, 400, 450\ nm$), and the material of the structure chosen to be silicon, so the added material is in homogenous with solar cell active material, and easy to fabricate. Further, the simulation temperature is set to be at room temperature 300 K, and the energy gap of the silicon active region is set to be (1.114eV) (35).

### 3.1. Optical Simulation Results

The effect of adding a rectangular substrate on reflection, absorption, and transmission spectra and prosed structure were noted in **Figure (3)**. It was shown that the transmission in all cases through the suggested solar cell is zero due to the Aluminum metal contact as seen in **Figure (1.b).**

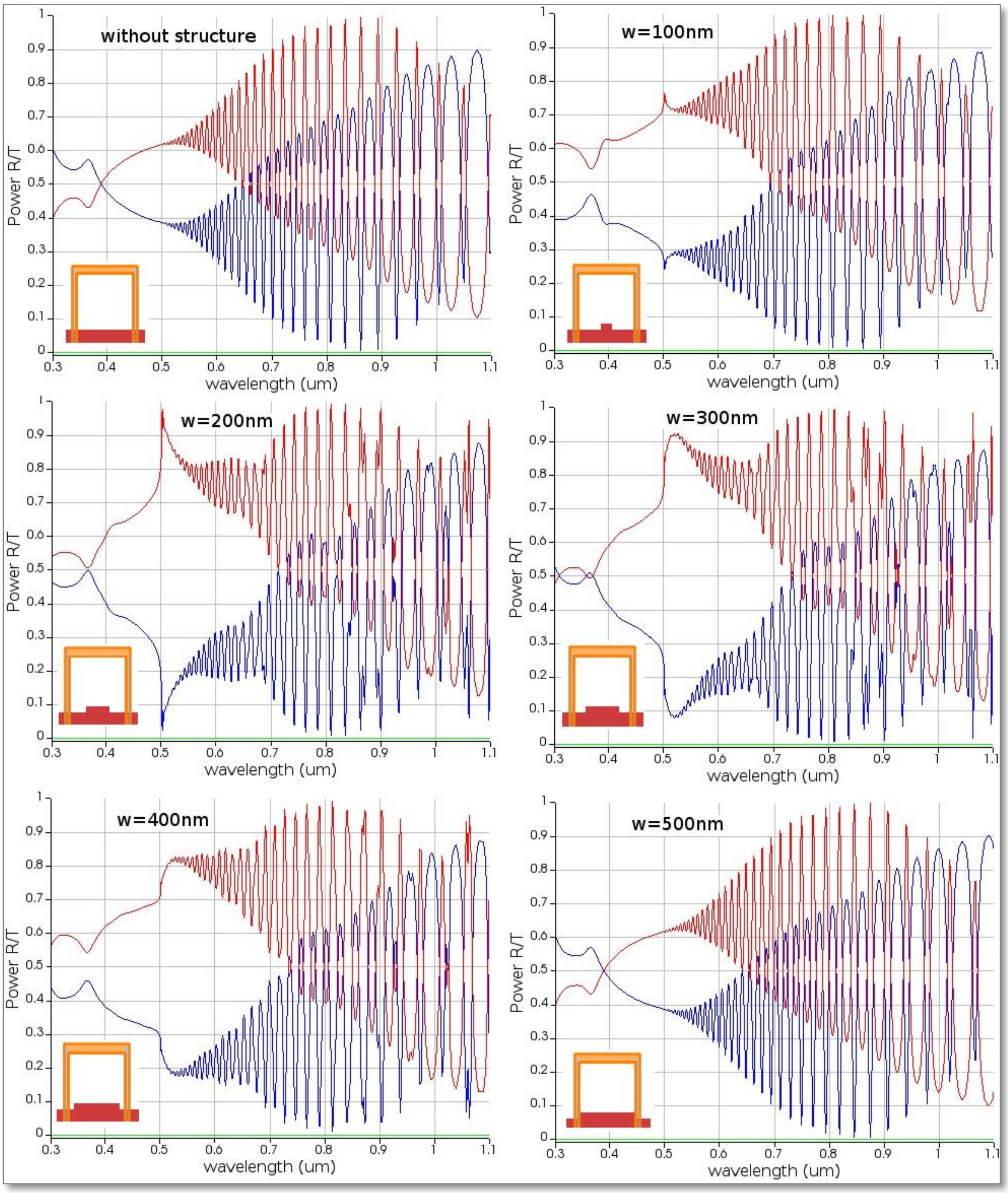


**Figure 3.** Reflection, Absorption, and Transmission spectra for different moth-eye structure widths: w= 0, 100, 200, 300, 400, and 500 nm, while the height of the structure was kept constant at h=50nm.

Furthermore, the ripples that appear in the absorption and reflection spectrum are caused by the Fabry-Perot resonant effect, which occurs inside a thin film solar cell with a metal base (36-38). It is also revealed from **Figure (3**) that there is a significant effect of adding structure on the reflection and transmission spectra. For example, in the case w=100nm, absorption increased relative to its initial values (without adding structure), and this absorption enhancement is clearer in the case w=200nm, and w=300nm. However, when the structure widths increased from 300nm to 400 nm, the corresponding absorption decreased. Further, when the structure width increased to 500nm, which means that the surface was covered completely with a silicon structure 50nm thick, the absorption decreased and became the same as the initial case (without adding structure).

**Figure (4**) represents the variation of absorption in case w=300nm with different values of structure height (h=0, 100, 200, 300, 400 nm). It is seen that the height of the structure has a significant effect on absorption, and the most absorption increase in visible region accords at height was (h=100nm) this absorption increased due to the maximization of the length of the optical path because of multiple reflection processes leading to confinement of the incident photons with the solar cell active layers (39, 40).

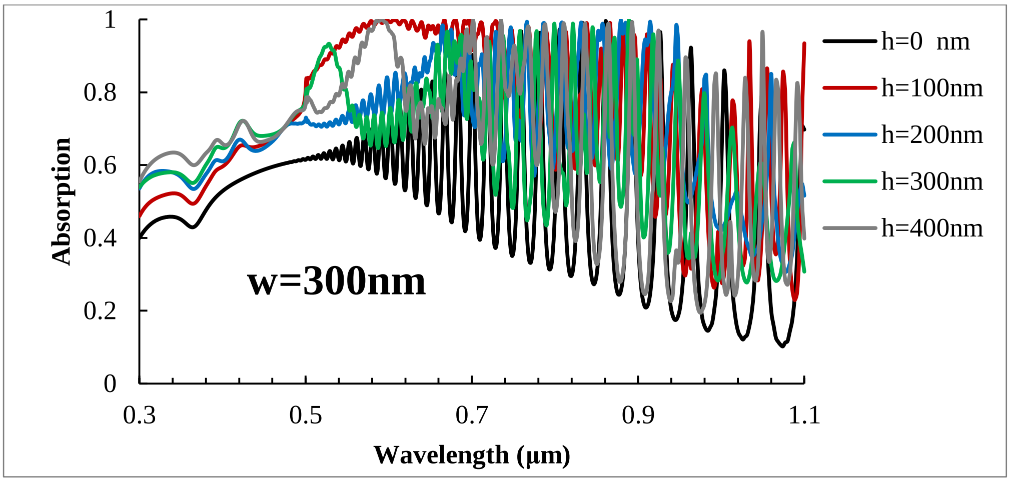


**Figure 4.** Absorption spectra for different moth-eye structure widths: w= 100nm, and different heights h= 0, 100, 200, 300, 400 nm.

### 3.2. Electrical Simulation Results

The electrical characteristics of the first suggested solar cell structure (w=100nm) for different structure heights are listed in **Table (1)**, It can be mentioned that the structure height significant effect on the solar cell short circuit current density $J_{sc}$, due to absorption enhancement, which leads to an increase in generation rate, the short circuit current increases from its initial value 17.19 $mA/cm^2$ to 19.19 $mA/cm^2$ at h=50nm, and then to a maximum value 21.42 $mA/cm^2$ at h=100nm. Meanwhile, $J_{sc}$ value decreases for higher structure height to 150, 200, 250 nm, and so on, due to the absorption decreases under these conditions. The maximum enhancement in current density was reported at a height of 100nm, which achieved about 24.4% of its initial value. Additionally, fill factor and open circuit voltage were slightly changed due to structure height variations, and the maximum value for both was achieved at h=100nm. Further, solar cell efficiency was enhanced from 8.71% to 10.98% at the case h=100nm due to the open circuit voltage, short circuit current, and fill factor.

**Table 1.** The impact of structure height on solar cell performance $J_{sc}, V_{oc}, FF, \eta$ at structure width w=100nm.

| High (nm) | $J_{sc}(mA/cm^2)$ | $V_{oc}(V)$ | FF | $\eta$ (%) |
|---|---|---|---|---|
| 0 | 17.1892 | 0.610627 | 0.829743 | 8.70914 |
| 50 | 19.191 | 0.614063 | 0.828713 | 9.76597 |
| 100 | 21.4248 | 0.616381 | 0.829932 | 10.9599 |
| 150 | 20.9735 | 0.61593 | 0.829458 | 10.7151 |
| 200 | 20.2093 | 0.61514 | 0.882879 | 10.3032 |
| 250 | 19.3177 | 0.614246 | 0.828648 | 9.83257 |
| 300 | 19.4848 | 0.614424 | 0.828664 | 9.92069 |
| 350 | 19.2034 | 0.614109 | 0.828695 | 9.77279 |
| 400 | 18.7793 | 0.61332 | 0.829008 | 9.54831 |
| 450 | 17.7391 | 0.611513 | 0.829565 | 8.99888 |

The effect of adding structure width is also investigated, **Table (2)** lists the short current density, and solar cell efficiency at different widths: 200, 300, and 400nm. It can be seen that there is similar behavior to the case w=100nm, the short circuit current increased gradually to a certain value of height which was h=100nm, and then it decreased after that certain value. As a result, the optimum design for the suggested rectangular structure with 300nm width and 100 nm height achieved an efficiency equal to 11.89 %, which means an efficiency enhancement of about 36.48%.

**Table 2.** The effect of structure height on $J_{sc}, \eta$ at structure widths: w=200, 300, 400nm.

| structure | Width w=200nm | | Width w=300nm | | Width w=400nm | |
|---|---|---|---|---|---|---|
| Height h (nm) | $J_{sc}$ $(mA/cm^2)$ | $\eta$ (%) | $J_{sc}$ $(mA/cm^2)$ | $\eta$ (%) | $J_{sc}$ $(mA/cm^2)$ | $\eta$ (%) |
| 0 | 17.189 | 8.709 | 17.189 | 8.709 | 17.189 | 8.709 |
| 50 | 19.632 | 9.998 | 19.867 | 10.122 | 19.366 | 9.856 |
| 100 | 22.584 | 11.588 | 23.132 | 11.886 | 21.886 | 11.209 |
| 150 | 21.697 | 11.108 | 21.664 | 11.089 | 20.075 | 10.233 |
| 200 | 19.832 | 10.104 | 19.626 | 9.996 | 18.376 | 9.335 |
| 250 | 18.484 | 9.392 | 17.650 | 8.951 | 17.342 | 8.789 |
| 300 | 17.903 | 9.086 | 17.417 | 8.829 | 16.738 | 8.470 |
| 350 | 17.566 | 8.907 | 16.898 | 8.555 | 16.076 | 8.121 |
| 400 | 17.584 | 8.917 | 16.288 | 8.233 | 15.782 | 7.965 |
| 450 | 17.243 | 8.737 | 15.402 | 7.764 | 15.450 | 7.790 |

**Figure (5)** represents the power density-voltage curves for the suggested four structures, It is clear that the best design (higher output power density) was achieved at (w=100nm) with a maximum output power density of about 11.89 $mW/cm^2$which represents an enhancement in the short circuit current density of about 34.57%.

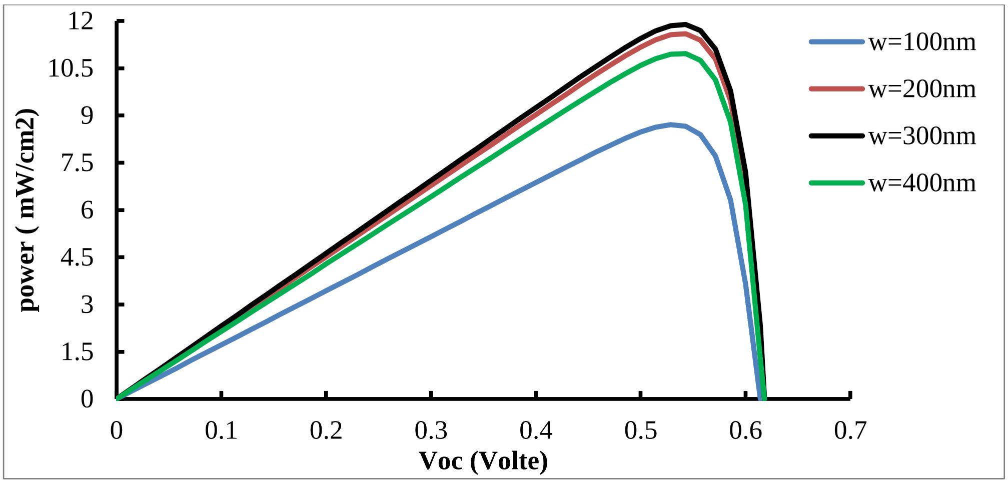


**Figure 5.** The power density-voltage curves for suggested structures.

The Current density-voltage characteristics curves for the suggested four structures are represented in **Figure (6)**. The maximum output current density achieved at w=300nm, with a maximum current density of about 23.13$mA/cm^2$

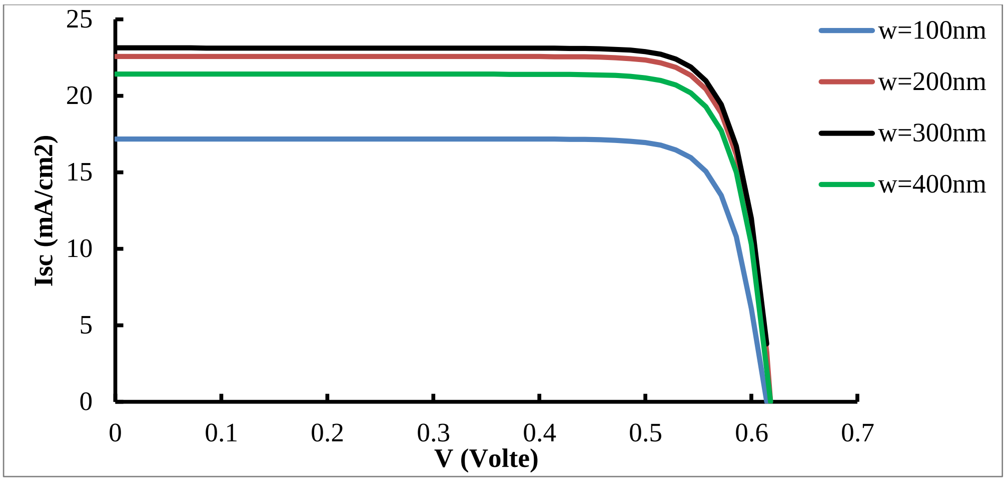


**Figure 6.** The Current density-voltage characteristics curve for the suggested structures.

**Figure (7)** shows the variation of the efficiency ($\eta$) as a function of the rectangle structure heights (0, 50, 100, 150, 200, 250, 300, 350, 400, 450nm) for the four structures design width (100, 200, 300, 400nm). It is obvious that, in each case, efficiency increases (from its initial value 8.709% ) gradually with increases in structure heights until it reaches its maximum values which are 10.960%, 11.589%, 11.886%, 11.209% respectively at a certain structure height which was (h=100nm), after that the efficiency decreases gradually.

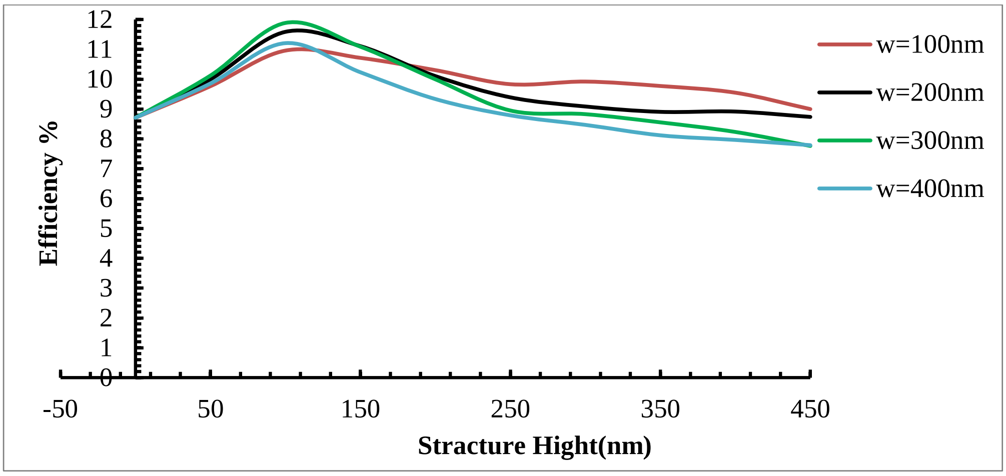


**Figure 7.** The Current density-voltage characteristics curves for suggested structures.

In fact, in each rectangle structure, there is an optimum design to achieve maximum improvements in ultra-thin film silicon solar cells, and the optimum improvement is achieved at a width of 300 nm, and 100nm in height.

## 4. Conclusion

This work considered rectangular silicon moth-eye structures with different dimensions to enhance silicon solar cell performance. The optical and electrical simulations show that the geometry of the introduced structure has a significant effect on suggested solar cell performance, with optimum enhancement achieved from 8.709% to 11.886% at a width of 300nm at a height of 100nm, we recommended introducing a more complex structure for additional performance enhancement, and it's helpful in use another optical design programs such as Silvaco, or SCAPS to develop the work in the future.

**Acknowledgment**

Thanks to the University of Baghdad, College of Education for Pure Science (Ibn Al-Haitham), Department of Physics.

**Conflict of Interest**

Not Found.

**Funding**

None.

**References**

1. Luo Y, Chen G, Chen S, Ahmad N, Azam M, Zheng Z, Su Z, Cathelinaud M, Ma H, Chen Z, Fan P, Zhang X, Liang G. Carrier transport enhancement mechanism in highly efficient antimony selenide thin-film solar cell. Adv Funct Mater. 2023;33(14):2213941. https://doi.org/10.1002/adfm.202213941
2. Chen X, Che B, Zhao Y, Wang S, Li H, Gong J, Chen G, Chen T, Xiao X, Li J. Solvent-assisted hydrothermal deposition approach for highly-efficient $Sb_2(S, Se)_3$ thin-film solar cells. Adv Energy Mater. 2023;13(21):2300391. https://doi.org/10.1002/aenm.202300391
3. Hassan Q, Viktor P, Al-Musawi TJ, Ali BM, Algburi S, Alzoubi HM, Al-Jiboory AK, Sameen AZ, Salman HM, Jaszczur M. The renewable energy role in the global energy transformations. Renew Energy Focus. 2024 Mar 1;48:100545. https://doi.org/10.1016/j.ref.2024.100545
4. Khaleel IH, Alkhafaji AA, Miran HA, Jaf ZN. Synthesis, characterization, photoluminescence, and antibacterial activities of silica-graphene oxide composites. Can J Phys. 2021;99(12):1105-1113. https://doi.org/10.1139/cjp-2020-0538
5. ElKhamisy K, Abdelhamid H, El-Rabaie ES, Abdel-Salam NA. Comprehensive survey of silicon thin-film solar cell: Challenges and novel trends. Plasmonics. 2024 Feb;19(1):1-20. https://doi.org/10.1007/s11468-023-01905-x
6. Kumar CM, Singh S, Gupta MK, Nimdeo YM, Raushan R, Deorankar AV, Kumar TA, Rout PK, Chanotiya CS, Pakhale VD, Nannaware AD. Solar energy: A promising renewable source for meeting energy demand in Indian agriculture applications. Sustain Energy Technol Assess. 2023 Feb 1;55:102905. https://doi.org/10.1016/j.seta.2022.102905
7. Roy P, Sinha NK, Tiwari S, Khare A. A review on perovskite solar cells: Evolution of architecture, fabrication techniques, commercialization issues and status. Sol Energy. 2020 Mar 1;198:665-688. https://doi.org/10.1016/j.solener.2020.01.080
8. Korany FM, Hameed MF, Hussein M, Mubarak R, Eladawy MI, Obayya SS. Conical structures for highly efficient solar cell applications. J Nanophotonics. 2018 Jan 1;12(1):016019. https://doi.org/10.1117/1.JNP.12.016019
9. Hasan AB, Ali MA. Improve performance of solar cell by using grooves which have semicircular shape on the surface by using program (ZEMAX). Ibn Al-Haitham J Pure Appl Sci. 2016;29(1). https://www.iasj.net/iasj/article/110873
10. Sarkara P, Pandab S, Majia B, Mukhopadhyay AK. Plasmon induced quantified agglomeration of $SiO_2$ nanoparticles to improve efficiency in solar cells. J Ovonic Res. 2022 Nov 1;18(6):723-730. https://chalcogen.ro/723_SarkarP.pdf
11. Pritom YA, Sikder DK, Zaman S, Hossain M. Plasmon-enhanced parabolic nanostructures for broadband absorption in ultra-thin crystalline Si solar cells. Nanoscale Adv. 2023;5(18):4986-4995. https://doi.org/10.1039/D3NA00436H
12. Al-Rubaiee M, Plaza GS. Optimizing the radius of curvature of black silicon peaks for solar cells using Matlab simulations. Iraqi J Sci. 2021 Dec 23;4272-7. https://www.iasj.net/iasj/download/5be01feb1a3f67d9

13. Matrood HM, Ail NT, Awaad AA. The effect of laser heating and overcasting deposition on the efficiency of plasmonic solar cell with noble metallic nanostructures. Iraqi J Sci. 2021 Dec 23;4240-8. https://www.iasj.net/iasj/download/08f7b150e33a2ce0
14. Abd Ali NN, Al-Agealy HJ, Moghaddam HM. Theoretical calculation of the fill factor of N749/[TiO]$_2$ solar cells. Ibn AL-Haitham J Pure Appl Sci. 2023 Oct 20;36(4):147-158 https://www.iasj.net/iasj/download/22fc86e45ab3bd4f
15. Assi AA, Saleh WR, Mohajerani E. Effect of deposit Au thin layer between layers of perovskite solar cell on cell's performance. Iraqi J Phys. 2021 Dec;19(51):23-32. https://www.iasj.net/iasj/download/1f53ab9ffc320a95
16. Amalathas PA, Alkaisi MM. Nanostructures for light trapping in thin film solar cells. Micromachines. 2019 Sep 17;10(9):619. https://doi.org/10.3390/mi10090619
17. Sellam M, Rasheed M, Azizii S, Saidani T. Improving photocatalytic performance: Creation and assessment of nanostructured $SnO_2$ thin films, pure and with nickel doping, using spray pyrolysis. Ceram Int. 2024 Jun 15;50(12):20917-20935. https://doi.org/10.1016/j.ceramint.2024.03.094
18. Khan MT. Unraveling the impact of graphene nanostructures passivation on the electrical properties of the perovskite solar cell. Mater Sci Semicond Process. 2023 Jan 1;153:107172. https://doi.org/10.1016/j.mssp.2022.107172
19. Saurabh S, Hossain MK, Singh S, Agnihotri SK, Samajdar DP. Optical performance analysis of InP nanostructures for photovoltaic applications. RSC Adv. 2023;13(15):9878-9891. https://doi.org/10.1039/D3RA00039G
20. Assi AA, Saleh WR, Mohajerani E. Effect of deposit Au thin layer between layers of perovskite solar cell on cell's performance. Iraqi J Phys. 2021 Dec;19(51):23-32. https://www.iasj.net/iasj/download/1f53ab9ffc320a95
21. Alesa HJ, Aldabbag BM, Salih RM. Natural pigment–poly vinyl alcohol nano composites thin films for solar cell. Baghdad Sci J. 2020 Sep 17;17(3):832-840. https://www.iasj.net/iasj/download/b87d682eb5a2b2fa
22. Ammar MH, Ons C, Ismail I. Promoting solar cell efficiencies via employing silver-carbon-pomegranate peel nanosystem. Baghdad Sci J. 2019;16(2). https://doi.org/10.21123/bsj.2019.16.2.0370
23. Jabbar MA, Alwan TJ. Design of anti-reflection coatings for application in the infrared region (10.6 microns). Iraqi J Sci. 2020 Nov 28;2897-2902. https://www.iasj.net/iasj/download/22e78630071955f9
24. Mahdi MA. Fabrication and characterization of silicon nanowires heterojunction solar cell. Iraqi J Phys. 2023 Sep 21;21(3):92-101. https://doi.org/10.30723/ijp.v21i3.1126
25. Hamdani AA. Experimental comparison for the performance of circular and square solar cells. Ibn AL-Haitham J Pure Appl Sci. 2017 Sep 22;21(1):24-30. https://jih.uobaghdad.edu.iq/index.php/j/article/view/1368
26. Rao KU, Reddy CA, Lakshmi GC, Vaishnavi G. Efficiency enhancement of the solar cells through subwavelength scaled biomimicked moth eye patterning using Lumerical solutions. Mater Today Proc. 2017 Jan 4;4(9):10407-10411. https://doi.org/10.1016/j.matpr.2017.06.389
27. Yuan Z, Li X, Jing H. Absorption enhancement of thin-film solar cell with rectangular Ag nanoparticles. J Appl Sci. 2014 Aug 14;14(8):823-827. https://scialert.net/abstract/?doi=jas.2014.823.827
28. Tabrizi AA, Pahlavan A. Efficiency improvement of a silicon-based thin-film solar cell using plasmonic silver nanoparticles and an antireflective layer. Opt Commun. 2020 Jan 1;454:124437. https://doi.org/10.1016/j.optcom.2019.124437
29. Rassekh M, Shirmohammadi R, Ghasempour R, Astaraei FR, Shayesteh SF. Effect of plasmonic aluminum nanoparticles shapes on optical absorption enhancement in silicon thin-film solar cells. Phys Lett A. 2021 Aug 27;408:127509. https://doi.org/10.1016/j.physleta.2021.127509
30. Mohsin AS, Mobashera M, Malik A, Rubaiat M, Islam M. Light trapping in thin-film solar cells to enhance the absorption efficiency using FDTD simulation. J Opt. 2020 Dec;49:523-532. https://doi.org/10.1007/s12596-020-00656-w

31. Anwar F, Afrin S, Satter SS, Mahbub R, Ullah SM. Simulation and performance study of nanowire CdS/CdTe solar cell. Int J Renew Energy Res. 2017 Jun 18;7(2):885-893. https://www.ijrer.org/ijrer/index.php/ijrer/article/view/5688
32. Kowsari A, Saghaei H. Resonantly enhanced all-optical switching in microfibre Mach–Zehnder interferometers. Electron Lett. 2018 Feb;54(4):229-231. https://doi.org/10.1049/el.2017.4056
33. Liu Y, Li Y, Wu Y, Yang G, Mazzarella L, Procel-Moya P, Tamboli AC, Weber K, Boccard M, Isabella O, Yang X, Sun B. High-efficiency silicon heterojunction solar cells: Materials, devices and applications. Mater Sci Eng R Rep. 2020 Oct 1;142:100579. https://doi.org/10.1016/j.mser.2020.100579
34. Palik ED. Handbook of optical constants of solids. Academic Press; 1998. Available from: https://shop.elsevier.com/books/handbook-of-optical-constants-of-solids/palik/978-0-08-053378-0
35. Dhaliah D, Xiong Y, Sipahigil A, Griffin SM, Hautier G. First-principles study of the T center in silicon. Phys Rev Mater. 2022 May;6(5):L053201. https://doi.org/10.1103/PhysRevMaterials.6.L053201
36. Eskandari M, Shamsi A. Absorption enhancement of ultra-thin film solar cells using Fabry-Perot and plasmonic modes. Phys Scr. 2023 Sep 18;98(10):105521. https://iopscience.iop.org/article/10.1088/1402-4896/acf52e/meta
37. Saravanan S, Dubey RS. Study of ultrathin-film amorphous silicon solar cell performance using photonic and plasmonic nanostructures. Int J Energy Res. 2022 Mar 10;46(3):2558-2566. https://doi.org/10.1002/er.7328
38. Oteki Y, Okada Y. External-quantum-efficiency enhancement in quantum-dot solar cells with a Fabry–Perot light-trapping structure. Heliyon. 2023 Aug 1;9(8). https://www.cell.com/heliyon/fulltext/S2405-8440(23)06520-9
39. Prashant DV, Agnihotri SK, Samajdar DP. Geometric optimization and performance enhancement of PEDOT: PSS/GaAs NP array based heterojunction solar cells. Opt Mater. 2021 Jul 1;117:111080. https://doi.org/10.1016/j.optmat.2021.111080
40. Shen X, Wang S, Zhou H, Tuokedaerhan K, Chen Y. Improving thin film solar cells performance via designing moth-eye-like nanostructure arrays. Results Phys. 2021 Jan 1;20:103713. https://doi.org/10.1016/j.rinp.2020.103713